2018 IEEE International Conference on Robotics and Automation (ICRA)
May 21-25, 2018, Brisbane, Australia

Kinematic Optimization of a Novel Partially Decoupled Three Degree of Freedom Hybrid Wrist Mechanism

Neil M. Bajaj and Aaron M. Dollar, *Member, IEEE*

***Abstract*— This paper discusses the kinematic design and geometric optimization of a novel hybrid three degree-of-freedom (DOF) wrist mechanism. The architecture consists of a one prismatic-revolute-universal linkage and one prismatic-spherical-spherical linkage in parallel with a revolute-universal linkage. This architecture is capable of spherical motion identical to that of a pitch-yaw-roll wrist. Moreover, this mechanism is considered to be partially decoupled, as not all actuators contribute to motion in an arbitrary direction. The forward and inverse kinematics of the parallel 2-DOF mechanism are presented. The 2-DOF mechanism is geometrically optimized over its design parameters to maximize a global transmission index, which measures the motion and torque transmissibility of particular wrist configuration over its workspace. The decoupled nature of the mechanism allows the pitch and yaw mechanism to be optimized separately, greatly reducing the parameter search space and allowing a much larger number of mechanism configurations to be simulated. We leverage this increase in simulated configurations to examine the effect of size constraints on the resulting mechanisms as well.**

I. Introduction

Within robotic manipulator systems, wrist devices serve to orient the end effector relative to the object or environment with which it interacts. However, many wrist devices tend to be lengthy serial chains, and their lack of compactness may make them unsuitable for some applications, such as prosthetic devices.

Parallel mechanisms alleviate some of the issues experienced with their serial counterparts, such as load isolation, high distal inertia, and size constraints, though they are generally more difficult to design and analyze. Moreover, parallel mechanisms often couple output DOFs to one another, requiring many actuators working in tandem to produce motion along a particular output DOF. Complexity of these mechanisms tends to increase with DOFs, further complicating design.

A hybrid parallel mechanism comprises both serial and parallel mechanisms, and can potentially confer the benefits of both types of mechanisms. For example, by using a single DOF rotator in series with a 2-DOF pointing mechanism, the roll capability of a mechanism may be greatly increased compared to a traditional parallel mechanism, such as in [1], where a hybrid mechanism utilizes a 2-DOF version of the Agile Eye and 1-DOF chain to increase roll compared to the Agile Eye [2]. The stiffness and bandwidth of the hybrid mechanism may also be greater than that of a comparable 3-DOF serial mechanism.

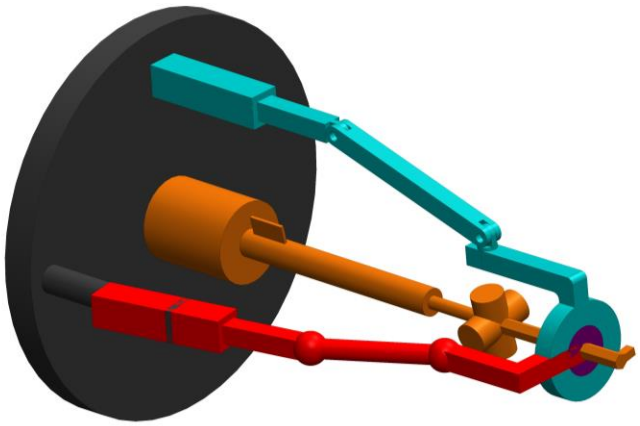

Fig. 1. Kinematic representation of the decoupled hybrid wrist

This paper presents the kinematic architecture and design of a 3-DOF hybrid wrist (Fig. 1) and details the optimization of the mechanism. The wrist is composed of a 2-DOF parallel pointing mechanism, which actuates the pitch and yaw DOFs of the end effector, and a single DOF serial mechanism that actuates roll. The mechanism is partially decoupled, meaning that the pitch, yaw, and roll values may be actuated sequentially, each with only a single actuator, to their desired positions (Fig. 2). However, actuating the pitch changes both the yaw and roll, and actuating the yaw changes the roll. This partial decoupling makes a single actuator largely responsible for a given output DOF, potentially allowing speed or torque requirements for each to be tailored individually, and for the sub-mechanisms to be analyzed separately. In terms of kinematics, the partial decoupling means that 3 off-diagonal elements of the displacement Jacobian are zero at all poses.

This mechanism is similar to a few others that have been presented in the literature. In [3], a fully decoupled 2 DOF wrist with similar architecture is presented, though the complete decoupling constrains the mechanism to having the same architecture of slider-cranks. In [4], a group of partially decoupled mechanisms is presented.

Hybrid mechanisms composed of a 2-DOF parallel mechanism and single DOF rotator in series have been applied to microsurgery [5], utilizing a 5 bar linkage and a single DC motor on the output link. An ankle/wrist system for humanoid robots was also developed based on hybrid architecture in [6], using an RU driven train to actuate roll. Similarly, In [7], a 2-DOF pointing mechanism was placed in parallel which a double universal joint rotator module.

This work was supported by the US Army Medical Research and Materiel Command, under contract W81XWH-15-C-0125. The authors are with the Department of Mechanical Engineering and Materials Science, Yale University, New Haven, CT 06511 (email: neil.bajaj@yale.edu; aaron.dollar@yale.edu).

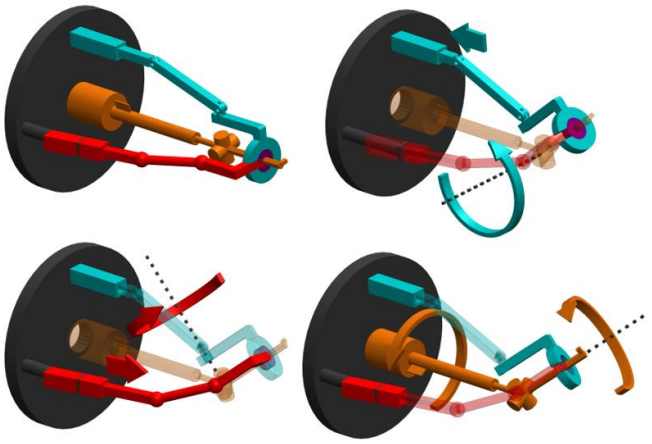

Fig. 2. Decoupled sequential actuation.

The optimization formulation described herein leverages the decoupling to allow the pitch and yaw mechanisms to be optimized individually, splitting the total parameter space into to two smaller spaces. Each of the smaller subspaces have lower dimensionality than the original space, which reduces the number of total mechanism combinations that need be simulated, as parameters of the pitch mechanism have no bearing on the workspace of the yaw mechanism. Thus, each can be sampled with finer resolution without increase of computational time. We optimize each mechanism for maximum average local transmission index [8] over the workspace, which takes both forward and inverse singularity into account. As the roll mechanism has no kinematic parameters, it is not included in this optimization procedure.

Within the optimization, we examine the effects of constraints of overall size parameters on the GTI, illustrate trends, and identify tradeoffs as a result of constraint.

We start with a description of the mechanism architecture, showing the forward and inverse kinematics to highlight the partial decoupling of output DOFs. Next, we discuss the optimization formulation, defining optimization metrics and constraints included in the simulations. We subsequently present the resulting optimal configuration of each sub-mechanism with a table of design parameters, and show the effect of tightening the size constraints on the resulting designs and optimality measure. We conclude with a discussion of the designs and future work.

II. Methods

A. Mechanism Architecture

The 3-DOF mechanism described in this paper is composed of a serial RU chain and a 2DOF parallel U, PRUR, PSSR (underline indicates actuated joint) mechanism. The U joint in the serial mechanism and the first U joint in the parallel mechanism are one and the same, and it serves as the center of the mechanism. Similarly, the final R joint on the parallel portion's legs corresponding to a bearing (purple in Fig. 1) that the end effector passes through. The 2-DOF mechanism can thus be considered to have a U, PRU, PSU architecture which controls pitch and yaw of the end effector, effectively "pointing" the roll axis in a particular direction. As such, the 2-DOF parallel mechanism will hereby be called the "pointing module", whereas the serial chain will simply be called the "roll module".

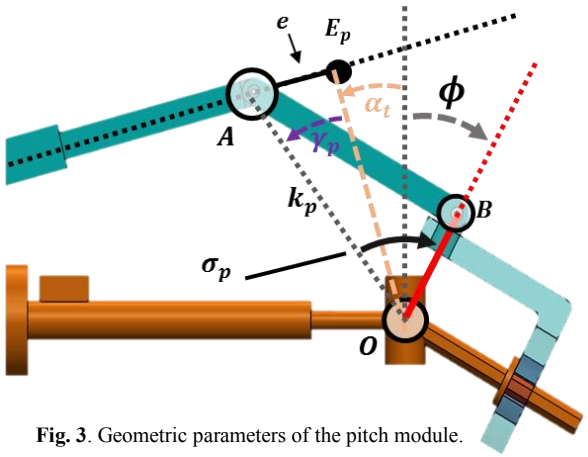

Fig. 3. Geometric parameters of the pitch module.

1) Pitch Module Kinematics

The pointing module can further be divided into a pitch module and a yaw module. The former is composed of the shared central U joint and the PRU chain. Actuating the P joint directly controls the pitch of the overall wrist. Furthermore, it may be simplified into a planar PRRR 4-bar linkage (Fig. 3) with all R joint axes coming out of the plane. The three R joints correspond to points ***A***, ***B***, and ***O.***

The central universal joint is replaced with the third R joint (at ***O***), and as the U joint within the PRU chain (at ***B***) has its second axis pointing directly to the center of the mechanism at all times, this axis may be ignored in the planar case. In truth, this second axis is the yaw axis of the wrist, which is why it must pass through the central U joint (to maintain pitch-yaw-roll spherical motion. In a 0° pitch position, this axis is parallel to the global z-axis. This leaves 4 parameters left to define the PRRR 4-bar (Fig. 3). Namely, these are r_p (minimum distance to P joint line of action, distance OE_p), α_p (angle from vertical to line of action), l_p (length of link AB), and r_B (distance OB).

The forward kinematics of the pitch module may be solved by isolating solvable triangles and using trigonometric laws. First, angle γ_p and distance k_p (Fig. 3b) must be determined from the actuator excursion e,

$$\begin{aligned} \gamma_p &= atan(e/r_p), \\ k_p &= sqrt(e^2 + r_p^2), \end{aligned} \tag{1}$$

where *atan*() is the arctangent function and *sqrt*() is the square root function. Note that e is a signed value which becomes negative when A is behind E_p. With k_p, we can then determine the angle σ_p (angle AOB) using law of cosines:

$$\sigma_p = acos((l_p^2 + r_p^2 - e^2 - r_p^2) / (l_p^* r_p)). \tag{2}$$

Summing the variety of angles centered at ***O*** yields an expression for the pitch angle ϕ:

$$\begin{aligned} \phi &= \alpha_p - \gamma_p - \sigma_p \ , \\ \phi(e) &= \alpha_p - atan(e/r_p) - acos((l_p^2 + r_p^2 - e^2 - r_p^2) / (l_p^* r_p)). \end{aligned} \tag{3}$$

This closed form expression can be differentiated to find the dexterity of the pitch module. Notice that the pitch angle is only a function of e and geometric parameters of the pitch module, indicating it is solely controlled by a single actuator.

The inverse kinematics of this linkage can be solved as well. Given the pitch angle ϕ, we can determine the excursion $\boldsymbol{e}$ by computing the intersection of a circle centered at the current position of $\boldsymbol{B}$ (defined by $\boldsymbol{\phi}$) with radius $\boldsymbol{l_p}$ and the P joint line of action (LOA). This intersection will be the location of $\boldsymbol{A}$. This generally results in two points, so to select one, we take the intersection point that keeps the intermediate link pointing in front of the P joint rather than behind. As this intersection point lies on the P joint LOA, we can easily compute e by simply measuring the distance between in and $\boldsymbol{E_p}$ and applying the proper sign as discussed previously.

2) Yaw Module Kinematics

The second half of the pointing module is the yaw module, which is composed of the central U joint and a PSS linkage. Though this is a spatial mechanism, its parameters can be defined in a planar view (Fig. 4a) for simplicity. This also ensures its workspace is symmetric about the midplane.

Five parameters define the linkage geometry. Namely, these are the P joint LOA minimum distance $\boldsymbol{r_s}$, the LOA angle from horizontal $\boldsymbol{\alpha_s}$, the length of intermediate link $\boldsymbol{GH}$ $\boldsymbol{l_s}$, and the two parameters which define the S joint at point $\boldsymbol{H}$, which are $\boldsymbol{h_x}$ and $\boldsymbol{h_x}$. The parameters $\boldsymbol{r_s}$ and $\boldsymbol{\alpha_s}$ define the location of point $\boldsymbol{E_s}$, which is the point on the LOA nearest to the origin. They also define the LOA direction vector $\boldsymbol{p_s}$.

As it is a 2-DOF mechanism, the yaw module requires two inputs to calculate the yaw angle θ via forward kinematics. One of these values is $\boldsymbol{e_s}$, the excursion of the P joint, and the other is the pitch angle $\boldsymbol{\phi}$. It can be seen in Fig. 4b that the pitch angle defines the plane that point $\boldsymbol{H}$, the second spherical joint must lie in. This is independent of the design of the pitch module, even though $\boldsymbol{\phi}$ is a function of $\boldsymbol{e}$. As a result, we may assume that the pitch angle is an external input to the yaw module, regardless of how the angle was achieved.

To compute θ given $\boldsymbol{e_s}$ and $\boldsymbol{\phi}$, we define a set of a set of geometric objects. We first define the yaw axis, which is fully determined by the pitch angle as it is constrained by a component of the pitch module. The axis $\boldsymbol{n(\phi)}$ is defined by a rotation of the unit $\boldsymbol{z}$ direction about the negative y-axis. The yaw axis and corresponding perpendicular plane, called the pitch plane, are defined by the following relationships:

$$\boldsymbol{n(\phi)} = [-sin(\boldsymbol{\phi}),\ 0,\ cos(\boldsymbol{\phi})]^T$$
$$\boldsymbol{X}^T \cdot \boldsymbol{n(\phi)} = \boldsymbol{0}, \quad (4)$$

where $\boldsymbol{X}$ is an arbitrary point in $\mathbb{R}^3$.

As e_s is an input to the system, we know the position of $\boldsymbol{G}$:

$$\boldsymbol{G}(\boldsymbol{e_s}) = \boldsymbol{E_s} + \boldsymbol{e_s} \cdot \hat{\boldsymbol{p}}_{\boldsymbol{s}} \quad (5)$$

The possible locations of $\boldsymbol{H}$ are limited to a sphere centered at $\boldsymbol{G}$ with radius $\boldsymbol{l_s}$. As $\boldsymbol{H}$ must also lie within the pitch plane, its possible positions are further limited to the circle $\boldsymbol{C_2}$ which results as an intersection of the aforementioned sphere and the pitch plane. This circle is centered at $\boldsymbol{G'}$, which is the projection of $\boldsymbol{G}$ into the pitch plane, and has a radius of

$$\boldsymbol{r_{c2}} = sqrt(\boldsymbol{l_s}^2 - (\boldsymbol{G} \cdot \boldsymbol{n}(\boldsymbol{\phi}))^2) \quad (6)$$

We can further limit the possible position of $\boldsymbol{H}$ to the circle $\boldsymbol{C_1}$, the circle of possible configurations given that $\boldsymbol{H}$ lies at a fixed position of the end effector. This circle also lies within the pitch plane, is centered at $\boldsymbol{O}$, and has radius

$$\boldsymbol{r_{c1}} = \text{sqrt}(\boldsymbol{h_x}^2 + \boldsymbol{h_y}^2). \quad (7)$$

As both circles $\boldsymbol{C_1}$ and $\boldsymbol{C_2}$ have known radii and lie within the pitch plane, their intersection can be easily computed. This once again yields two intersection points, and we choose the point in front of the P joint along its LOA, and call it point $\boldsymbol{J}$. To calculate θ from $\boldsymbol{J}$, we use the following relationship

$$\boldsymbol{\theta} = atan2(sgn(\boldsymbol{J_x}) \cdot sqrt(\boldsymbol{J_x}^2 + \boldsymbol{J_z}^2), \boldsymbol{J_y}) + atan2(\boldsymbol{h_x}, \boldsymbol{h_y}). \quad (8)$$

The relationship between θ and inputs $\boldsymbol{e_s}$ and $\boldsymbol{\phi}$ can be derived algebraically via substitution of many of the previous expressions, though is excluded here for brevity.

Inverse kinematics of the yaw module are similar to those of the pitch module. After specifying θ and $\boldsymbol{\phi}$, the position of $\boldsymbol{H}$ is fully specified. A sphere with radius $\boldsymbol{l_s}$ is centered at this point, and the intersection between this sphere and the P joint LOA can be determined, which results in two possible locations of $\boldsymbol{G}$. Using Eqn. (5), we may solve for $\boldsymbol{e_s}$ and pick the solution that results in $\boldsymbol{H}$ in front of $\boldsymbol{G}$ along the LOA.

3) Roll Module

The roll module is composed to a simple RU serial chain. The kinematics of this type of chain are well known and can be seen in [9]. As there are no geometric design parameters of this mechanism which affect the kinematics, it does not need to be optimized.

The kinematics of this chain do depend on the pitch and yaw angles θ and $\boldsymbol{\phi}$, which define a total "bend" angle for the U joint. This bend angle affects the relative phasing between

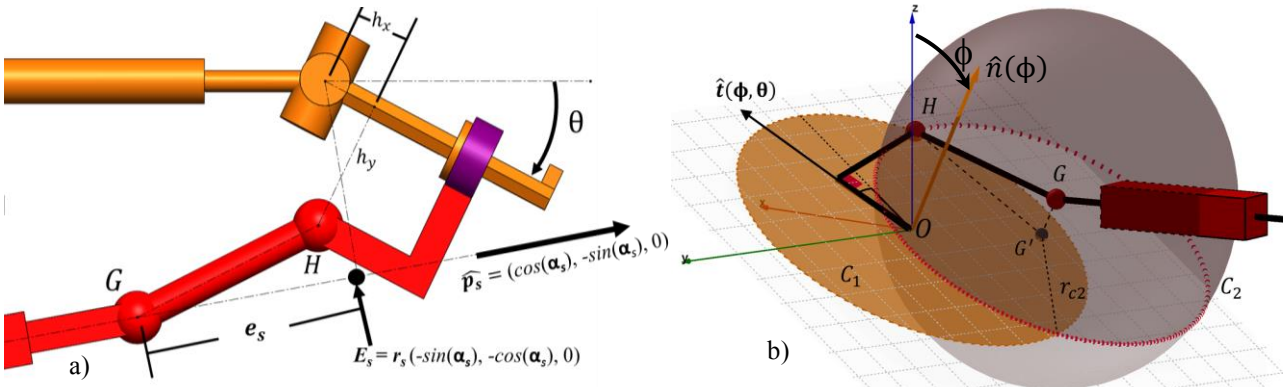

Fig. 4. a) Kinematic parameters of the yaw module S. Note the yaw angle θ is measured positive counterclockwise. (pictured value is negative). b) Sphere-circle intersection in forward kinematics. Note the point $\boldsymbol{G'}$ is the point $\boldsymbol{G}$ projected into the pitch plane, which perpendicular to $\boldsymbol{n(\phi)}$ and passing through the origin $\boldsymbol{O}$.

input and output rotation, and this phasing is changed as the bend angle varies.

4) Jacobian

As previous sections on the kinematics have shown, the pitch DOF is only controlled by a single actuator, yaw by two, and roll is affected by all three. This gives the Jacobian a structure of

$$\boldsymbol{J}(\boldsymbol{\phi},\boldsymbol{\theta},\boldsymbol{\psi}) = \begin{bmatrix} \frac{d\boldsymbol{\phi}}{d\boldsymbol{e}} & 0 & 0 \\ \frac{\mathrm{d}\boldsymbol{\theta}}{\mathrm{d}\boldsymbol{e}} & \frac{d\boldsymbol{\theta}}{d\boldsymbol{e_s}} & 0 \\ \frac{d\boldsymbol{\psi}}{d\boldsymbol{e}} & \frac{d\boldsymbol{\psi}}{d\boldsymbol{e_s}} & \frac{d\boldsymbol{\psi}}{d\boldsymbol{e_r}} \end{bmatrix}, \qquad (9)$$

where $\boldsymbol{\psi}$ is the output roll and $\boldsymbol{e_r}$ is the input roll actuator in the RU chain.

B. Simulation and Optimization

1) Simulation Structure

In order to find the optimal design of the hybrid wrist mechanism, we opt to simulate both the pitch and the yaw modules over their workspaces with a large number of different parameter combinations. For the 1-DOF pitch mechanism, we set a desired workspace of 50º in either direction (100 º total) from the neutral position, though for clarity of results we extend the simulated workspace to 60 º either way. The inverse kinematics described previously are used to sample 65 uniformly spaced points over the 120 º workspace, and determine if the particular point is reachable with the given configuration.

The same approach is taken for the yaw module, except the workspace is a 2-DOF space of pitch and yaw. The extended workspace is a 120 º by 120 º section uniformly sampled by a 65x65 point grid. The desired workspace is a circle centered at 0° pitch and yaw with a radius of 50°.

To explore the design space of the modules, we vary the kinematic parameters using exhaustive combination. To avoid simulating configurations which are dilated versions of a previous configuration, we force the linear parameters to sum to 1 and always be positive. This forces the linear parameters to fall within the unit simplex, which is then sampled by the algorithm described in [10]. Using the simplex constraint also nondimensionalizes the configurations, allowing for unitless comparison.

As shown in the forward kinematics section, the fact that the parameters of the pitch module do not affect the yaw module and vice versa makes the mechanism partially decoupled. As such, instead of simulating al combinations of all 9 design parameters, we may simulate and optimize the pitch module over its 4 kinematic parameters without exhaustive combination with all configurations of the yaw mechanism. For the same number of total configurations, a 4 DOF space and a 5 DOF space may be sampled much more finely (less distance between samples) than a 9 DOF space.

2) Optimization Metrics

To compare various configurations of the modules with one another, we compute a series of metrics during the simulation. The most important metrics we consider are the transmission indices described in Wang et al [8]. In particular, these indices are called the input transmission index (ITI) and the output transmission index (OTI). Each of these indices are calculated at each point in the workspace of the module, which makes them local metrics. They are defined as

$$\boldsymbol{ITI_i} = |\$_{Ti} \cdot \$_{Ii}| \,/\, |\$_{Ti} \cdot \$_{Ii}|_{max} \qquad (10)$$
$$\boldsymbol{OTI_i} = |\$_{Ti} \cdot \$_{Oi}| \,/\, |\$_{Ti} \cdot \$_{Oi}|_{max},$$

where $\$_{Ii}$ is the input twist screw (ITS) of the ith leg (motion of the actuator in said leg), $\$_{Oi}$ is the output twist screw (OTS, the motion allowable when all actuators but the one in the ith leg are locked), and $\$_{Ti}$ is the transmission wrench screw (TWS) of the ith leg (unit wrench the ith leg applies to the end effector).

With both mechanisms, the ITI is simply the inner product of the P joint LOA unit vector and the unit axial direction of the intermediate link. This index corresponds to power transfer when the P joint is actuated with unit velocity, and resisted by unit axial force on the intermediate link. As it is normalized by the theoretical maximum, the ITI is simply the cosine of the angle between these two vectors. In this case, it approaches zero near workspace boundaries.

For the OTI, we define $\$_{Oi}$ slightly differently, as this is not a fully parallel manipulator. Instead of using the unconstrained DOF of the platform, for the pitch module, we use the y axis as $\$_{Oi}$, and we use the axis $\boldsymbol{n(\phi)}$ for the yaw module. Using these, the OTI reduces to the percentage of maximal theoretical torque about this specified axis, with unit force applied by the intermediate link. The OTI approaches zero near points of torque singularity. The local transmission index (LTI) is defined as the minimum of the ITI and OTI at a given workspace point.

It should be noted that other popular metrics for optimization of parallel mechanisms may not be appropriate here. Using isotropy measure such as those in [11] would require the two mechanisms to be simulated simultaneously. Using dexterity as defined in [12] would also require tandem information of both mechanisms. Moreover, simply maximizing the Jacobian determinant would result in configurations with high speed ratios but low torque. See [13] for a comprehensive discussion on metrics.

Unlike in [14], instead of ranking configuration by the percentage of the desired workspace above a certain LTI threshold, we opt to average the LTI over the desired workspace, as our objective is not to maximize the good transmission workspace. This average LTI value is the Global Transmission Index (GTI).

We also consider sizing metrics within this optimization. Firstly, we look at the minimum distance the intermediate link achieves from the origin or negative x-axis, and call this value d_{min}. We also look at the maximum distance the intermediate link reaches from only the origin, and call this value d_{max}. These constraints are related to clearance from the center axis and total size, respectively. They both may limit the compactness of a given physical design. If d_{min} is too small, the mechanism must be expanded until it has enough central clearance. If d_{max} is too large, then some components may not be able to be shrank far enough to reach absolute size constraint. We look at the effect of having these metrics act as constraints on the GTI.

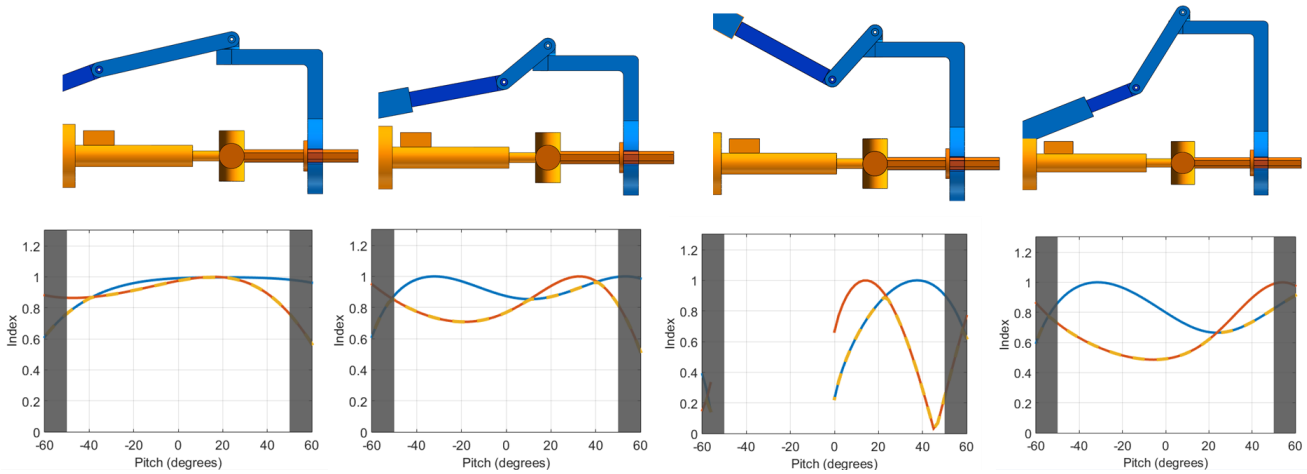

Fig. 5. Resulting configurations and associated LTI of pitch module configurations. In each LTI graph, the blue line corresponds to ITI, red to OTI, and the yellow dashed line to LTI, which is the minimum of the two at any pitch angle. a) O.C., highest GTI configuration, b) V2, high GTI configuration with better constraint satisfaction (in d_{min}), c) V3, very high d_{min}, low GTI configuration, d) V4, low d_{max} , low d_{min} configuration, moderate GTI.

III. Results

As each module was optimized independent of one another, we present the resulting optimal designs of each of the resulting mechanisms and show the effects of constraints on the GTI.

A. Pitch Module

Using the parameter space sampling method from and previous sections, we simulated 5,177,200 different configurations of the four design parameters of the pitch module. Inverse kinematics were used to simulate the workspaces of these mechanisms at a set of uniformly spread discrete points. Of these configurations, there were 2,021,486 that produced a feasible geometry that could reach at least a portion of the desired workspace.

The optimal configuration (henceforth called O.C.), that maximized the GCI is shown in blue in the lower half of Fig. 5a, with the yaw mechanism components omitted. The specific local values of the ITI and OTI, shown over the extended workspace for clarity, can be seen in the upper half of Fig. 5a. Table I lists the parameters and metrics of the various configurations presented.

The O.C. is the best possible performer when no constraints on d_{min} and d_{max} are enforced. In Fig. 6, we may see the effect of changing these two constraints on the GTI. Obviously, the O.C. would satisfy any constraints which require lower d_{min} or higher d_{max} (relaxing constraints) than its own. This corresponds to moving to the upper left from the O.C. However, tightening these constraints will result in new configurations with lower GTI. However, the region near the O.C. is rather flat, and constraints may be tightened without significant loss in performance. In general, the OC is much closer to the best possible d_{max} performance than the best possible d_{min} performance. Configuration V_2 (Fig. 5b) has a slightly lower GTI than the O.C., similar d_{max}, but satisfies much tighter d_{min} constraints.

A variety of constraint combinations do result in feasible configurations with high GTI, evidenced by the large red area in Fig. 6. Tightening the constraints on d_{max} results in gradually decreasing GTI, down to values around GTI ≈ 0.5, after which it sharply drops to 0. The right side of this plot corresponds to increasing the required d_{min} of a configuration, up to a boundary of $d_{min} \approx 0.325$. between V_2 and V_3 (Fig. 5c). This boundary continues upward past V_3, though with less steep performance loss when $d_{max} > 0.8$. Between V_2 and V_4 (Fig. 5d), the boundary is an interaction between both constraints, possibly indicating a tradeoff between which satisfiable constraints in this region. Between these points, it is roughly approximated by $d_{max} = 0.5*d_{min} + 0.45$.

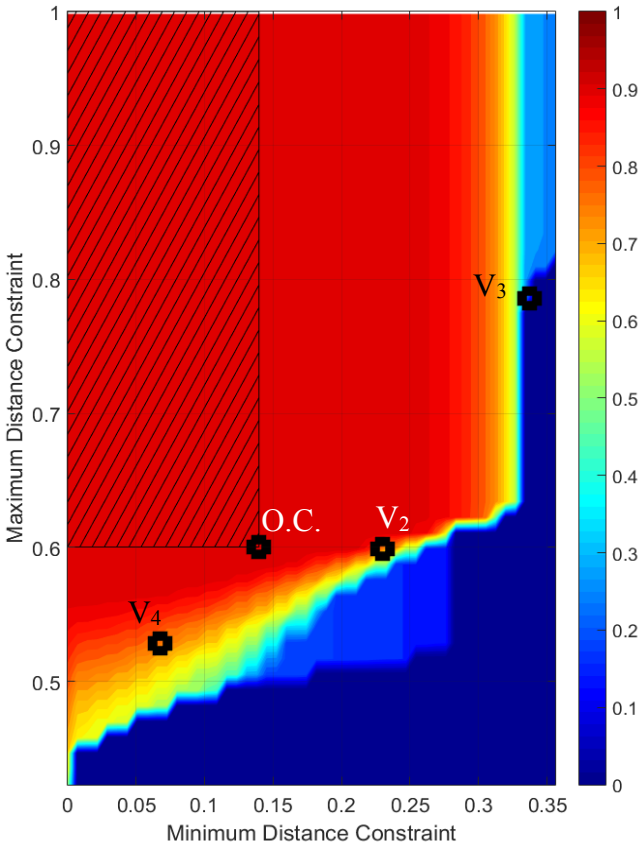

Fig. 6. Effect of constraints on GTI. The hatched region upper-left of O.C. corresponds to no possible improvements by relaxing constraints. Moving downwards and to the right correspond to tightening d_{max} and d_{min} constraints, respectively.

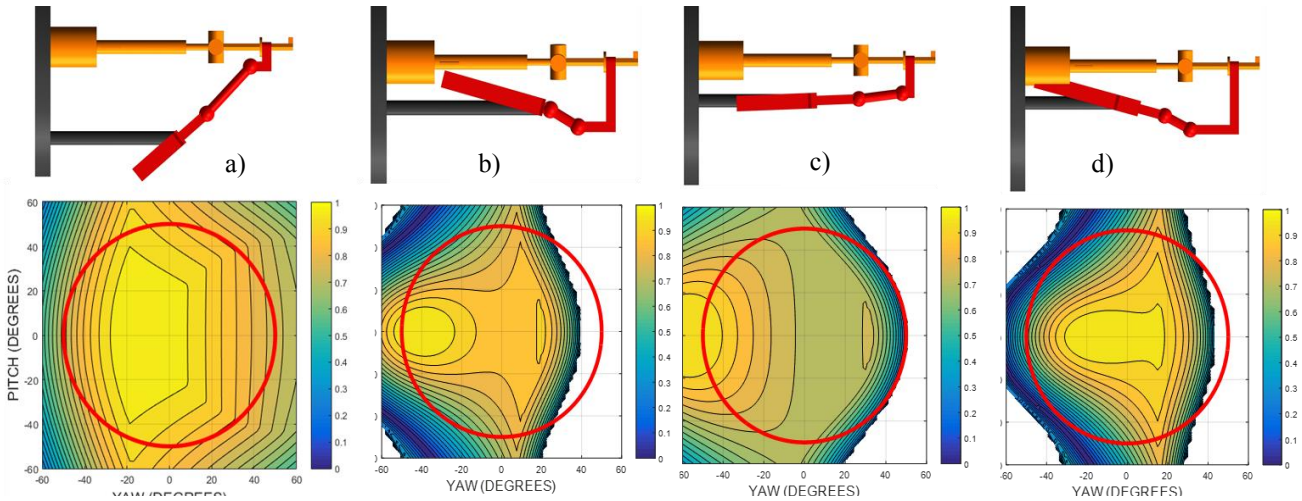

Fig. 7. Resulting configurations and associated LTI for yaw module. In each LTI graph, a) O.C., highest GTI configuration, b) W_2, GTI > 0.7 with better constraint satisfaction, c) W_3, lowest d_{max} configuration with GTI > 0.7, d) W_4, highest d_{min} configuration with GTI > 0.7.

Notably, configuration V_3 shows two types of singularities that may occur in the mechanism's workspace. Near the neutral position around 0º, the intermediate link is perpendicular to the actuator line of action, meaning velocity of the input actuator will not result in linkage output motion. This corresponds to the ITI being 0. Around 40º, the intermediate link becomes colinear with a line radially extending from the central U joint. This corresponds to the linkage being able to create no torque on the platform. This corresponds to a value of 0 in the OTI.

The kinematic geometry of configuration V_4 leads to interference of the pitch module with the roll module. The mechanism could be physically designed to avoid this interference issue without changing the kinematics, though at the expense of greater complexity and more components. This could be achieved by offsetting the P joint parallel to its line of action.

Note that many configurations for this mechanism are geometrically limited in d_{min} by the parameter r_B, which is the upper maximum d_{min} any configuration may have. It is also the lower limit for d_{max}, but its values which appear for d_{max} do not appear to be close to the limit. Having a larger r_B can theoretically allow for higher d_{min}, but due to the simplex constraint, other linear parameters would have to decrease. Decreasing the length of the intermediate link requires it to reach steeper angles relative to the P joint LOA, which may reduce ITI.

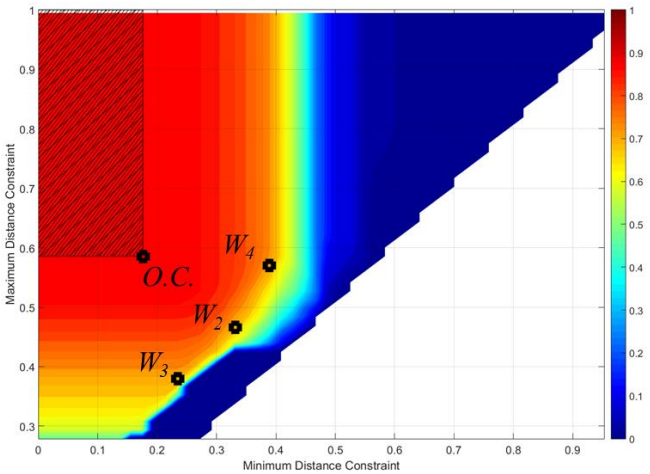

Fig. 8. Effect of constraints on GTI on the yaw module. The hatched region upper-left of O.C. corresponds to no possible improvements by relaxing constraints. Moving downwards and to the right correspond to tightening d_{max} and d_{min} constraints, respectively. The boundary on the right corresponds to impossible configurations (d_{max} <d_{min}).

TABLE I. PITCH MODULE CONFIGURATIONS

Conf.	r_p	l_p	r_b	α_p	GTI	d_{min}	d_{max}
O.C	0.335	0.358	0.307	0.356	0.922	0.140	0.600
V_2	0.327	0.227	0.446	0.185	0.812	0.230	0.599
V_3	0.214	0.257	0.529	-0.499	0.272	0.337	0.786
V_4	0.266	0.268	0.466	0.413	0.600	0.077	0.493

B. Yaw Module

Though the yaw module is only directly responsible for actuating the yaw DOF, its kinematics are affected by the pitch angle, and thus is simulated as a 2DOF mechanism. In total, 3,359,960 configurations were simulated, and 1,582,192 were able to reach a portion of the required workspace.

The O.C., as well as other configurations, may be seen in Fig. 7 with the pitch module suppressed. Their associated LTI plots only shown the minimum transmission index at each point in the workspace. The extended workspace corresponds to region within the red circle.

Similar to the pitch mechanism, we can explore the role of sizing constraints on the GTI and examine the resulting suboptimal mechanisms. Fig. 8 shows that constraints affect the yaw module differently than the pitch module. Note the large white region to the right corresponds to configurations with d_{min} larger than d_{max}, which impossible to satisfy.

While a sharp boundary does exist near W_3, where performance quickly deteriorates to 0 as constraints are tightened in either direction. However, for the rest of the region of feasible configurations, the GTI gradually decreases toward 0 as constraints are tightened. The contours corresponding to constant GTI appear to be composed of portions where each constraint limits the GTI independently and a smaller region where they interact, between W_2 and W_3.

The configurations W_3, is the configuration with the smallest d_{max} possible while keeping GTI above 0.7. Similarly, W_4 has the largest d_{min} with GTI above the same limit. W_2 has the same GTI constraint and is chosen to be to

the lower right of the O.C. From Fig. 7, it is clear that reducing the GTI this low reduces the reachable workspace of the mechanisms compared to the OC. Nominally, this could be remedied by lengthening the intermediate link, but the constraint of linear parameters summing to 1 would mean that the new mechanism would have lower d_{min}. When comparing the O.C. to W_2, we find a much larger d_{min} (twice as large), but when looking at the actual configuration of the two in Fig. 7, we can see that d_{min} does increase, but the distance to the central axis of the wrist becomes much smaller.

TABLE II. YAW MODULE CONFIGURATIONS

Conf.	r_s	l_s	r_{sy}	r_{sx}	α_s	GTI	d_{min}	d_{max}
O.C.	0.277	0.408	0.120	0.195	0.698	0.889	0.176	0.586
W_2	0.332	0.201	0.372	0.095	-0.257	0.704	0.332	0.466
W_3	0.245	0.295	0.211	0.249	0.037	0.713	0.235	0.380
W_4	0.397	0.194	0.406	0.003	-0.257	0.719	0.389	0.570

IV. DISCUSSION

A. Effects of Constraints

1) Pitch Module

From Figs. 5 and 6, we can see that the pitch module can satisfy constraints and maintain high GTI with d_{min} <0.325 and d_{max} > 0.5, and tradeoffs between d_{min} and d_{max} by the boundary near the OC and configurations V2 and V4. Outside of this region, performance can fall sharply. Increasing the d_{min} (e.g. V_3) simply results in configurations which cannot access a large part of the workspace, which is the region where the intermediate link would become perpendicular to the P joint line of action. On the other hand, decreasing d_{max} (e.g. V_4) results in geometries that require links to cross the central axis of the wrist and introduce output singularities, where the producible torque approaches 0. In physical implementation, it impossible to actuate through a torque singularity in the absence of external torques, so the reachable workspace would generally be smaller than the workspace derived via inverse kinematics.

2) Yaw Module

The corresponding figures of the yaw module show that outside of a relatively flat region of $d_{min} < 0.3$ and $d_{max} > 0.5$, performance falls nearly linearly with decreasing d_{max}. However, increasing d_{min} causes performance to fall much more quickly, reaching GTI < 0.10 by $d_{min} = 0.5$. Interestingly, the GTI does not reach 0 immediately after this point, but rather slowly decays toward the infeasibility boundary.

Given the yaw module has two linear parameters which form the upper limit for d_{min} for a given configuration, it is surprising that it can achieve similar performance boundaries to the pitch module as d_{min} increases. This upper limit on d_{min} is minimal when $\boldsymbol{h_x} = \boldsymbol{h_y}$. From Fig. 7b and d, it is clear that the two configurations with highest d_{min} (W_2 and W_4) have relatively large $\boldsymbol{h_y}$ compared to $\boldsymbol{h_x}$. Combined with the P joints being angled outwards, thee both appear to serve to increase d_{min}. These factors also seem to limit configurations from reaching the far edge of the desired workspace ($\theta > 40°$).

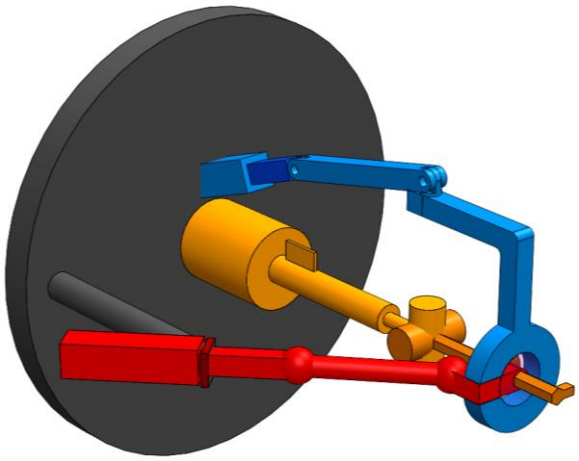

Fig. 9. Optimal configurations of the pitch and yaw modules combined. The pitch module has been scaled so that its sum on linear parameters sums to 12.5cm, whereas the yaw module sums to 10cm.

B. Combining Modules

Though optimized separately, the physical implementation of the mechanism shall have both the pitch and yaw modules incorporated. As their optimizations were unitless, a size scale for each would need to be determined for fabrication. In this case, the pitch module has higher d_{min} and d_{max} than the yaw module. If clearance issues were more critical, the yaw module could be scaled larger than the pitch module (e.g., pitch module linear parameters sum to 10 cm while yaw parameters sum to 12.5 cm). The pitch module could also be scaled down by the same ratio if reducing d_{max} is more important.

Fig. 9 shows the resulting O.C.s combined into a single mechanism. The pitch module's d_{min} is about 25% less than the yaw module. If we stipulate that greater center clearance is better, then scaling the simplex of the pitch module parameters to 12.5cm and the yaw module parameters to 10cm should maintain the same higher d_{min}, as it was limited by the yaw module. Their values of d_{max} are approximately equal before scaling, so scaling the pitch module up by 25% will increase the mechanism's total d_{max} to 7.5cm as opposed to 5.9cm. However, to avoid interference with the central roll mechanism, the top mechanism's P joint would have to be offset upwards already.

In the case where one module outperforms the other in both size factors, then either one factor would have to be the poorer performer, or the tradeoff between GTI and satisfying constraints could be leveraged. Compared to the pitch module, the more gradual decrease and overall wider range of satisfiable constraints allows for greater freedom to trade-off size for performance in the yaw module. This is especially the case if large tradeoffs must be made.

Other factors not accounted for within this optimization framework may also drive the size scales. Torque requirements, packaging or fabrication of small components, and general strength and robustness may require that a module be scaled up to meet demands, even if the other module can be sized smaller. On the other hand, actuation length limitations for the prsimatic joints and actuation speed may

require a module be scaled down. Having areas of little GTI change is beneficial for more than pure constraint matching requirements.

V. Conclusion

In this paper, we have presented the design of a novel hybrid 3-DOF parallel wrist mechanism. The architecture is partially decoupled, which allows us to optimize parts of the sub-mechanisms independently, and then recombine them post optimization. We present the forward and inverse kinematics as well as an optimization scheme for searching the parameter space. We looked at the effect of optimizing under size constraints on the GTI and how the constraints affect the resulting configurations. Boundaries for how far a constraint may be tightened are examined, and configurations at those boundaries are presented.

VI. References

[1] T. A. Hess-Coelho, "A Redundant Parallel Spherical Mechanism for Robotic Wrist Applications," *J. Mechanical Design*, Vol. 129, no. 8, p. 891, 2007.

[2] C. M. Gosselin, E. St. Pierre, and M. Gagné, "On the Development of the Agile Eye," *IEEE Robotics and Automation Magazine*, vol. 3, no. 4, pp. 29–37, Dec-1996.

[3] M. Carricato and V. Parenti-Castelli, "A Novel Fully Decoupled Two-Degrees-of-Freedom Parallel Wrist," *Int. J. Robotics Research*, vol. 23, no. 2000, pp. 661–667, 2004.

[4] Q. Jin and T.-L. Yang, "Synthesis and Analysis of a Group of 3-Degree-of-Freedom Decoupling Parallel Manipulators," *Proc. ASME Des. Eng. Tech. Conf. MECH-34240*, vol. 126, no. March 2004, pp. 2–9, 2002.

[5] A. Degirmenci, F. L. Hammond, J. B. Gafford, C. J. Walsh, R. J. Wood, and R. D. Howe, "Design and Control of a Parallel Linkage Wrist for Robotic Microsurgery," in *IEEE International Conference on Intelligent Robots and Systems*, 2015, pp. 222–228.

[6] S. Alfayad, F. B. Ouezdou, and F. Namoun, "New 3-DOFs Hybrid Mechanism for Ankle and Wrist of Humanoid Robot: Modeling, Simulation, and Experiments," *J. Mech. Des.*, vol. 133, no. February 2011, p. 21005, 2011.

[7] F. L. Hammond III, R. D. Howe, and R. J. Wood, "Dexterous High-Precision Robotic Wrist for Micromanipulation," in *16th International Conference on Advanced Robotics*, 2013.

[8] J. Wang, C. Wu, and X. J. Liu, "Performance evaluation of parallel manipulators: Motion/force transmissibility and its index," *Mechanism and Machine Theory*, vol. 45, no. 10, pp. 1462–1476, 2010.

[9] A. Mills, "Robert Hooke's 'universal joint' and its Application to Sundials and the Sundial-Clock," *Notes Rec. R. Soc.*, vol. 61, no. 2, pp. 219–236, 2007.

[10] N. Smith and R. Tromble, "Sampling uniformly from the Unit Simplex," *Johns Hopkins Univ. Tech. Rep*, no. 2, pp. 1–6, 2004.

[11] D. Chablat and P. Wenger, "Architecture Optimization of a 3-DOF Translational Parallel Mechanism for Machining Applications, the Orthoglide," *IEEE Transactions on Robotics and Automation*, vol. 19, no. 3, pp. 403–410, 2003.

[12] T. Yoshikawa, "Manipulability of Robotic Mechanisms," *Int. Journal of Robotics Research*, vol. 4, no. 2, pp. 3–9, 1985.

[13] J. P. Merlet, "Jacobian, Manipulability, Condition Number, and Accuracy of Parallel Robots," *Journal of Mechanical Design*, vol. 128, no. 1, p. 199, 2006.

[14] C. Wu, X.-J. Liu, L. Wang, and J. Wang, "Optimal Design of Spherical 5R Parallel Manipulators Considering the Motion/Force Transmissibility," *Journal of Mechanical Design*, vol. 132, no. 3, p. 31002, 2010.